Supplementary Information

Confined phase transition triggering high-performance energy storage thermo-battery

Jing Li, Shiyan Chen*, Xiangyang Qu, Zhiliang Han, Zhou Zhou, Lili Deng, Yuhang Jia, Shengming Zhang, Ruimin Xie and Huaping Wang*

State Key Laboratory for Modification of Chemical Fibers and Polymer Materials, College of Materials Science and Engineering, Donghua University, Shanghai 201620, PR China

E-mail: chensy@dhu.edu.cn, wanghp@dhu.edu.cn

Note S1. Theoretical analysis of the thermopower

There is a hypothetical temperature-dependent reversible redox reaction between A and B (aA + ne$^-$ ↔ bB) in a thermos-electrochemical cell (TEC). The Seebeck coefficient (Se) was calculated as the ratio of the potential difference (ΔE) to temperature difference (ΔT), according to Eq. 1:[1, 2]

$$Se = \frac{\Delta E}{\Delta T} = \frac{E_H - E_C}{T_H - T_C} \quad (1)$$

where E_H and E_C are the potential at the hot and cold sides of the sample, respectively. And T_H and T_C are the temperature at the hot and cold electrodes of TEC, respectively.

According to the Nernst equation, for above mentioned redox reaction (aA + ne$^-$ ↔ bB), the equilibrium potential (E) can be expressed as:

$$E = E^0 + \frac{RT}{nF} \ln \frac{(a_A)^a}{(a_B)^b} \quad (2)$$

where E^0 is the standard potential, F is the Faraday constant, R is the ideal gas constant, a_A and a_B are the activities of species A and B, respectively. The activity (a) is defined as the product of the activity coefficient (γ) and concentration (C) (a = γ × C).

$$E = E^0 + \frac{RT}{nF}\left[\ln \frac{(\gamma_A)^a}{(\gamma_B)^b} + \ln \frac{(C_A)^a}{(C_B)^b}\right] \quad (3)$$

According to Eq. 1, Se can be finally written as the sum of two terms:

$$Se = \frac{R}{nF\Delta T}\left[T_H \ln \frac{(\gamma_A)_H{}^a}{(\gamma_B)_H{}^b} - T_C \ln \frac{(\gamma_A)_C{}^a}{(\gamma_B)_C{}^b}\right] + \frac{R}{nF\Delta T}\left[T_H \ln \frac{(C_A)_T{}^a}{(C_B)_T{}^b} - T_C \ln \frac{(C_A)_C{}^a}{(C_B)_C{}^b}\right] \quad (4)$$

Excess free enthalpy (G^E) refers to the difference between the real solution properties and the ideal solution free enthalpy properties under the same conditions of temperature, pressure and composition ($G^E = \Delta G - \Delta G^{id}$). The G^E value is proportional to its γ.

$$G^E = RT \sum C_i \ln \gamma_i \quad (5)$$

where ΔG is the Gibbs free energy, ΔG^{id} is Gibbs free energy of ideal solution.

In general, ΔG is calculated by:

$$\Delta G = \Delta H - T\Delta S \quad (6)$$

Phase transition is characterized as a discontinuous and abrupt change in volume, solubility, or molecular conformation of a material at its transition temperature.[3] The formation or dissolution of the precipitates is induced in a much narrower temperature region during a phase transition. Assuming that ΔH is constant under the temperature

region which can be estimated from isothermal titration calorimetry.[4, 5]

$$\ln \gamma \propto -\Delta S \tag{7}$$

For the TEC containing the equal–concentration I^-/I_3^- aqueous electrolyte ($I_3^- + 2e^- \leftrightarrow 3I^-$) with a certain amount of methylcellulose (MC) under the open-circuit state, when the hot electrode temperature is below the gelation temperature of MC, both concentrations of the redox species on the hot and cold sides are equal, that is, $\Delta C = 0$. In this case, *Se* is only related to the entropy difference of the redox reaction. Hence, the second term of Eq. 4 can be neglected, and *Se* can be simplified as:

$$Se = \frac{R}{2F\Delta T}\left[T_H \ln \frac{\left(\gamma_{I_3^-}\right)_H}{(\gamma_{I^-})_H^3} - T_C \ln \frac{\left(\gamma_{I_3^-}\right)_C}{(\gamma_{I^-})_C^3}\right] \tag{8}$$

Here, it is worth noting that the definition of *Se* is defined as positive sign in this work.

When the hot electrode temperature is above the gelation temperature of MC, the hydrophobic interaction between MC and I_3^- ions leads to a substantially reduced I_3^- concentration at the hot side ($\Delta C \neq 0$).[6] Thus, Eq. 4 is expressed as:

$$Se = -\frac{R}{2F\Delta T}\left[T_H \ln \frac{\left(\gamma_{I_3^-}\right)_H}{(\gamma_{I^-})_H^3} - T_C \ln \frac{\left(\gamma_{I_3^-}\right)_C}{(\gamma_{I^-})_C^3}\right] - \frac{R}{2F\Delta T}\left[T_H \ln \frac{\left(C_{I_3^-}\right)_H}{(C_{I^-})_H^3} - T_C \ln \frac{\left(C_{I_3^-}\right)_C}{(C_{I^-})_C^3}\right] \tag{9}$$

According to Eq. 9, the first term is considered to be dominated by difference in entropy (ΔS) between the redox anions,[7, 8] the second term is only related to the concentrations of A and B (ΔC).

$$\frac{1}{\Delta T}\left[T_H \ln \frac{\left(\gamma_{I_3^-}\right)_H}{(\gamma_{I^-})_H^3} - T_C \ln \frac{\left(\gamma_{I_3^-}\right)_C}{(\gamma_{I^-})_C^3}\right] \propto \Delta S \tag{10}$$

$$\frac{1}{\Delta T}\left[T_H \ln \frac{\left(C_{I_3^-}\right)_H}{(C_{I^-})_H^3} - T_C \ln \frac{\left(C_{I_3^-}\right)_C}{(C_{I^-})_C^3}\right] \propto \Delta C \tag{11}$$

On the contrary, *Se* here has opposite sign compared to the one mentioned above Eq. 8.

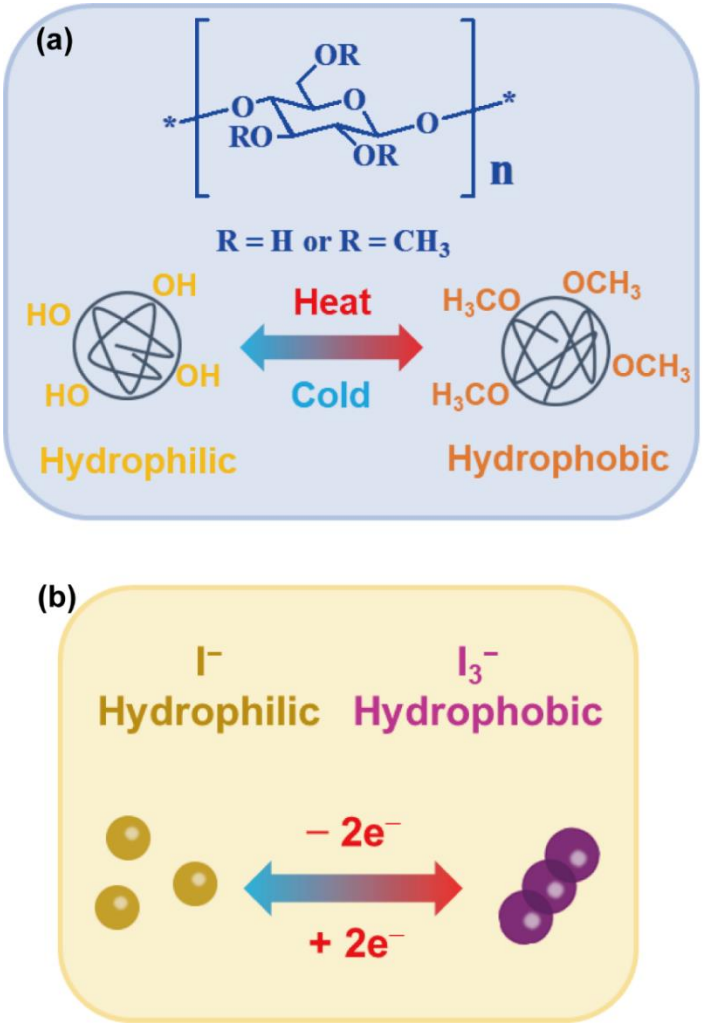

Fig. S1 The molecular structure and properties of (a) MC and (b) I^- and I_3^- ions.

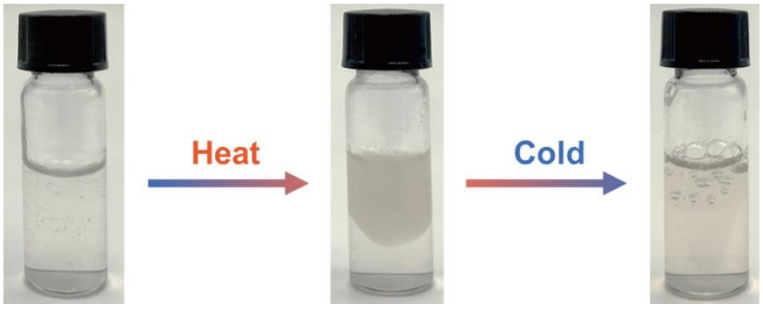

Fig. S2 Photograph of 2 wt% MC electrolyte upon heating and cooling.

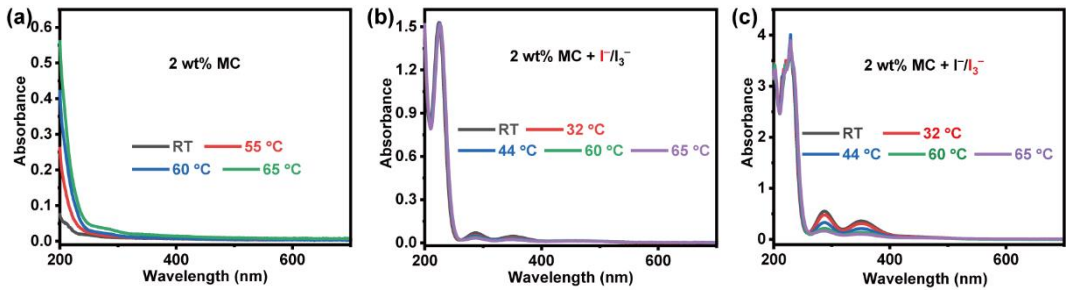

Fig. S3 UV-Vis spectra of 2 wt% MC diluted 25 times (a), 2 wt% MC + I^-/I_3^- diluted to 2×10^{-5} M (b), and 2 wt% MC + I^-/I_3^- diluted to 10^{-4} M (c) in the electrolyte at different temperatures. The peak at 225 nm is assignable to the I^- ion, and the peaks at 288 and 352 nm are assigned to I_3^- species dissolved in deionized water. This dilution concentration refers to the I^-/I_3^-solution.

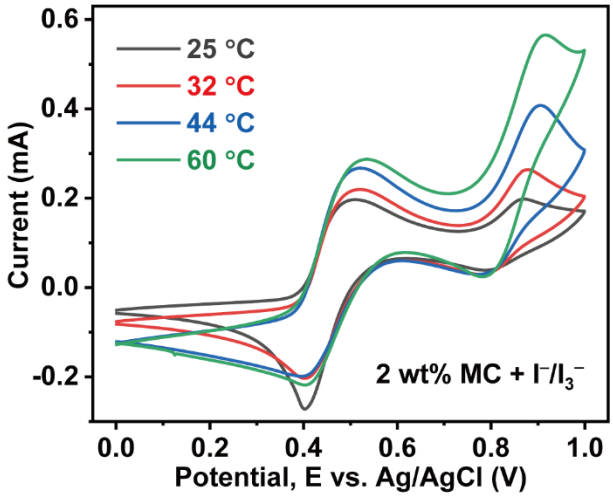

Fig. S4 CV curves of 2 wt% MC + I^-/I_3^- electrolyte with increasing temperature.

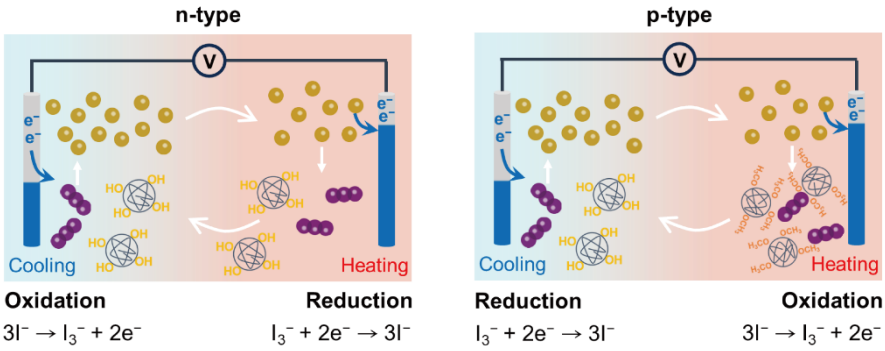

Fig. S5 Schematics of n-type TEC and p-type thermo-battery for I^-/I_3^- redox couple induced by MC.

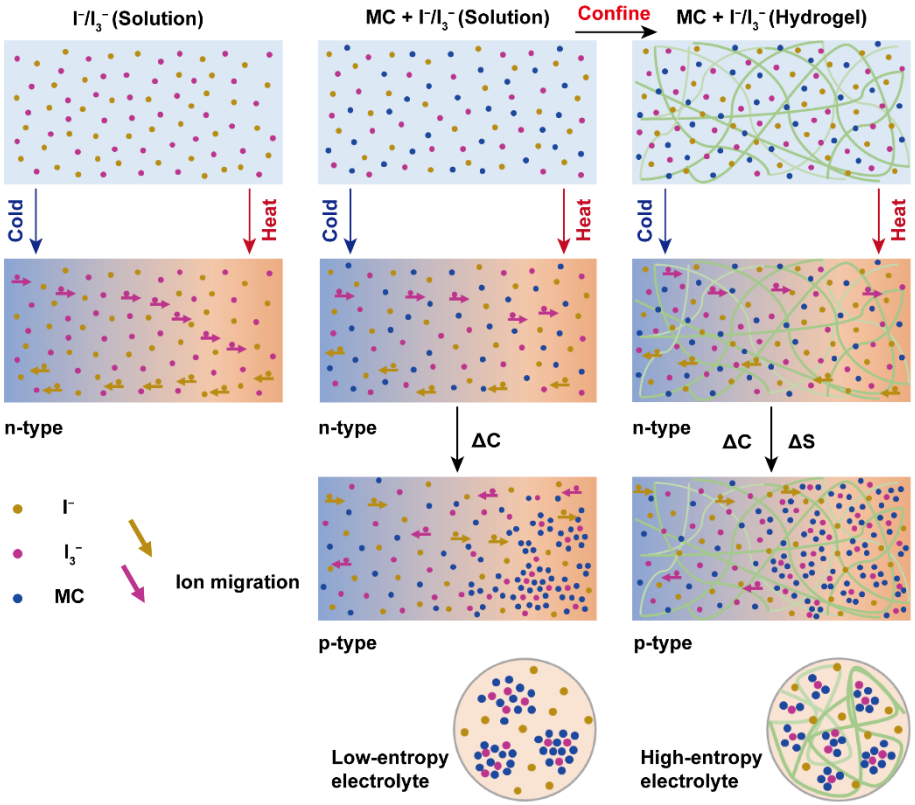

Fig. S6 Design concept of thermo-batteries and schematic of enhanced thermopower**.** Low-entropy electrolyte refer to the electrolyte system with a weak solvation interaction between the I_3^- ions and H_2O. In contrast, high-entropy electrolyte refers to the electrolyte system with a strong solvation interaction between I_3^- ions and H_2O, which has smaller ion clusters.

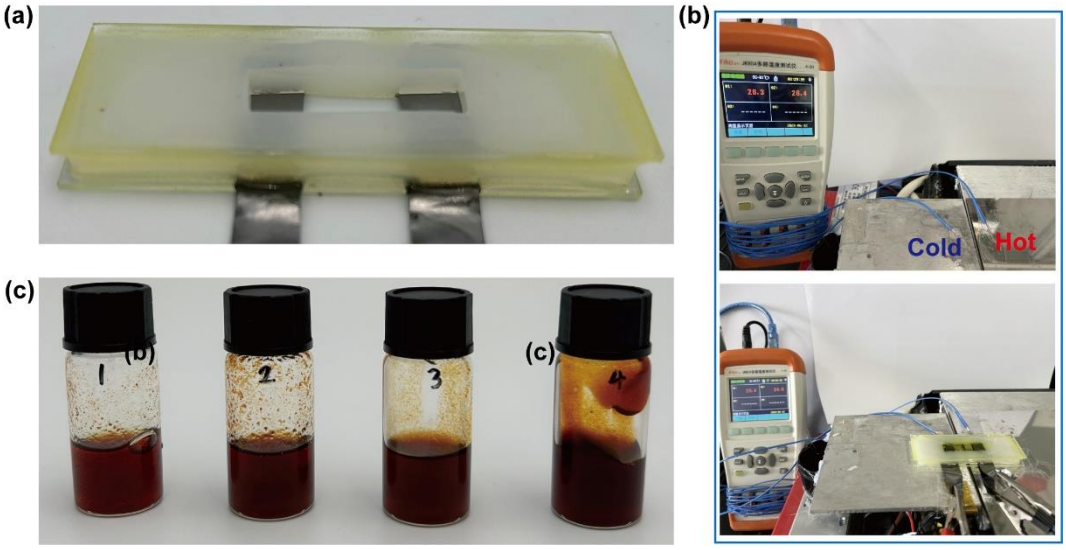

Fig. S7 (a) Experimental setup for characterizing the thermopower and power

generation performance. (b) The photos of the home-made equipment. (c) Photograph of x wt% MC + I^-/I_3^- electrolytes (x = 1, 2, 3, 4) from left to right. The electrolytes become more viscous with the increase of MC content.

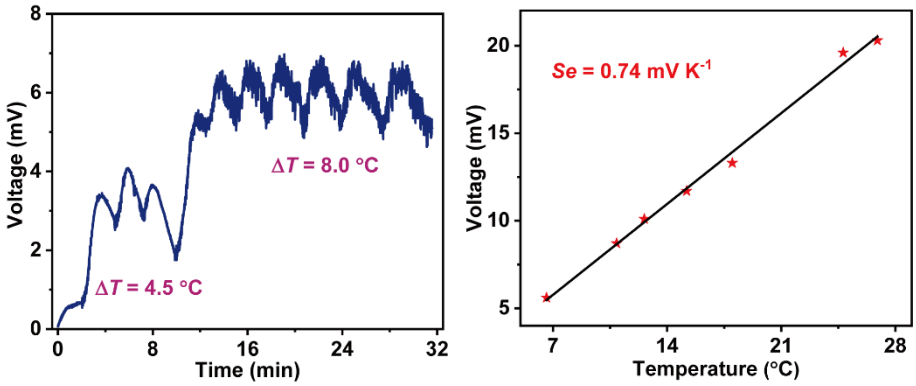

Fig. S8 Recorded open-circuit voltage over time and *Se* of the thermocell with I^-/I_3^- electrolyte.

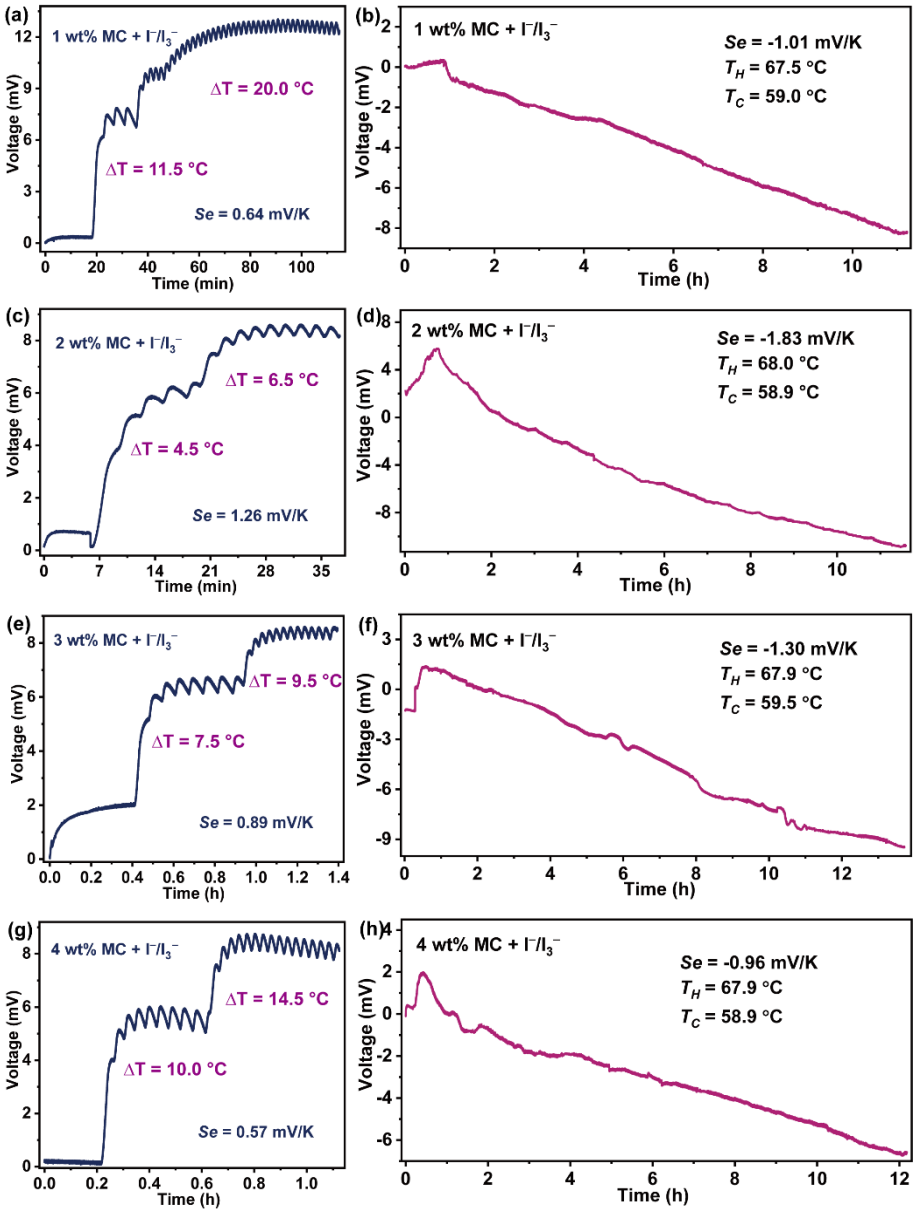

Fig. S9 Recorded open-circuit voltages for (a) 1, (c) 2, (e) 3, and (g) 4 wt% MC + I^-/I_3^- electrolytes of n-type thermocells and for (b) 1, (d) 2, (f) 3, and (h) 4 wt% MC + I^-/I_3^- electrolytes of p-type thermo-batteries. And T_H is held at room temperature for n-type themocell.

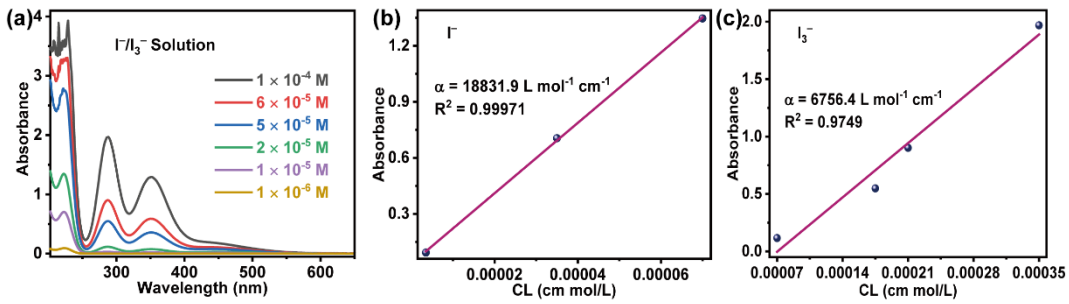

Fig. S10 (a) UV-Vis spectra of I^-/I_3^- solutions with a series of concentration gradients. The fitting of molar extinction coefficient of (b) I^- at 225 nm, and (c) I_3^- at 288 nm based on the absorbance at different concentrations. The thickness of the solution is 3 cm in the cuvette.

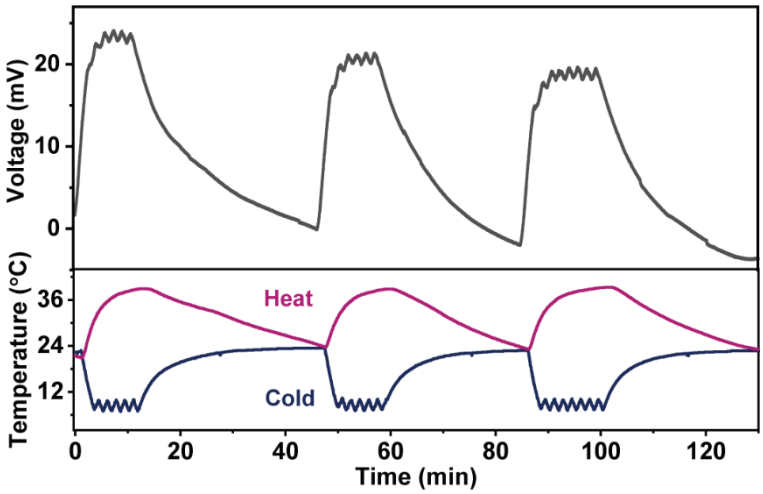

Fig. S11 The open-circuit voltage-time curves of I^-/I_3^- electrolyte with and without temperature difference.

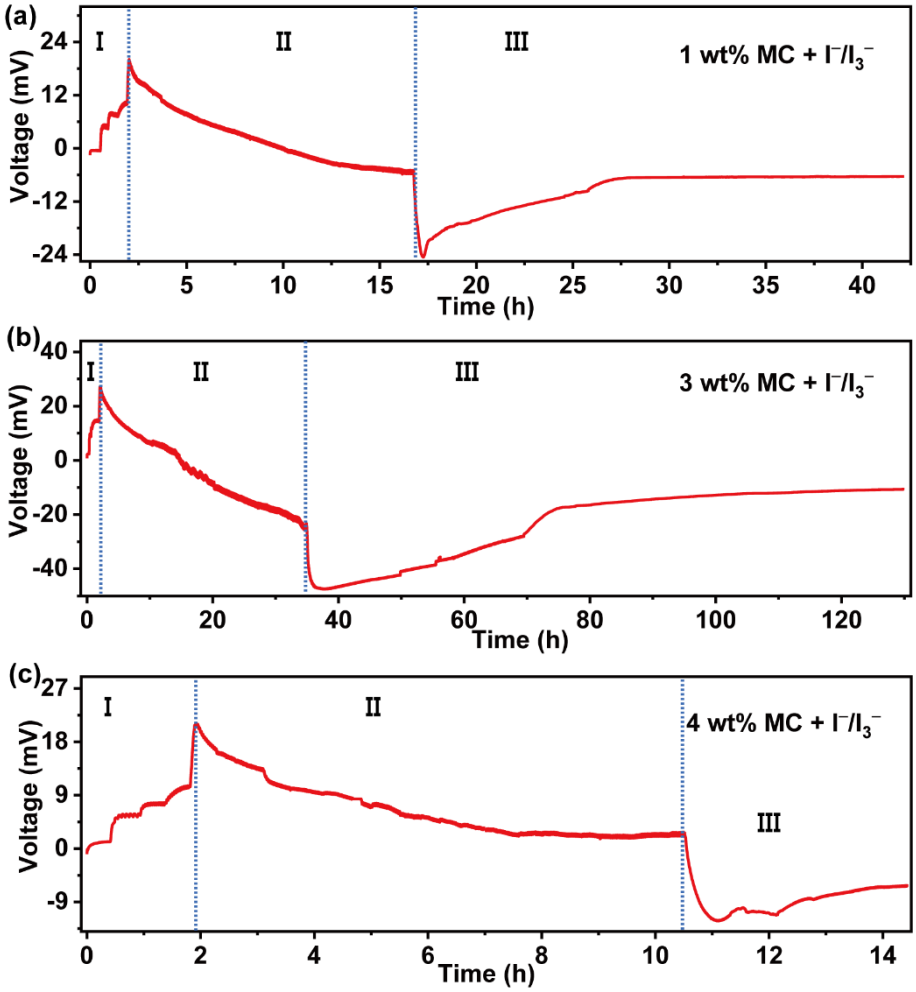

Fig. S12 Recorded open-circuit voltages for (a) 1, (b) 3 and (c) 4 wt% MC + I^-/I_3^- electrolytes during charging and self-discharging (I: $T_H < 56$ °C, n-type; II: $T_H > 56$ °C, p-type; III: $\Delta T = 0$ °C, the V_{OC} decreases slowly), The cold electrode temperature is held at 15 °C.

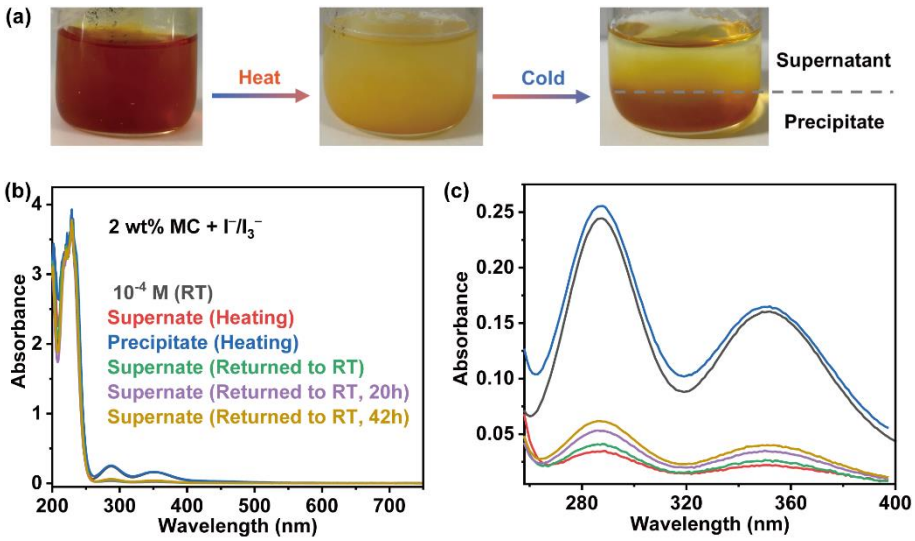

Fig. S13 (a) Photographs of 2 wt% MC + I^-/I_3^- electrolyte under different temperatures, and the schematic showing the change of MC from the hydrophobic to hydrophilic state upon heating and cooling. (b) UV-Vis spectra of the 2 wt% MC + I^-/I_3^- electrolytes with different treatment conditions, and magnified UV-Vis spectra (c) of wavelengths from 258 to 400 nm.

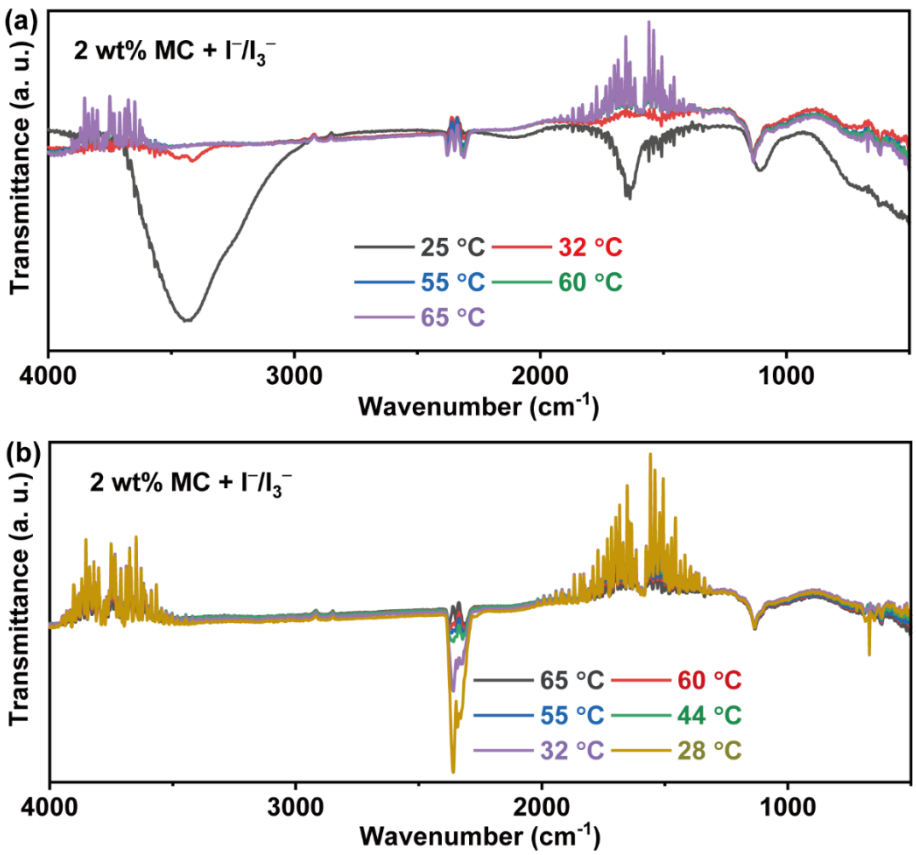

Fig. S14 FTIR spectra about 2 wt% MC + I^-/I_3^- electrolyte solution in a closed heating (a) and cooling (b) cycle.

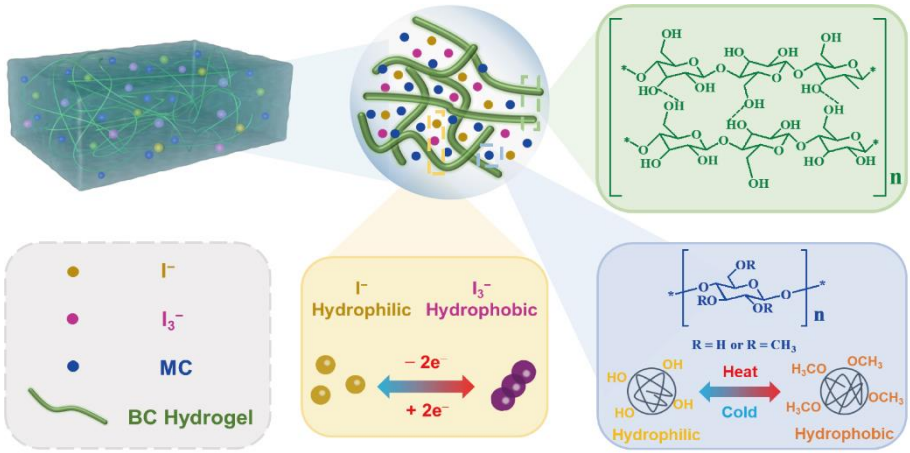

Fig. S15 Components of BC hydrogel-based 2 wt% MC + I^-/I_3^- electrolyte.

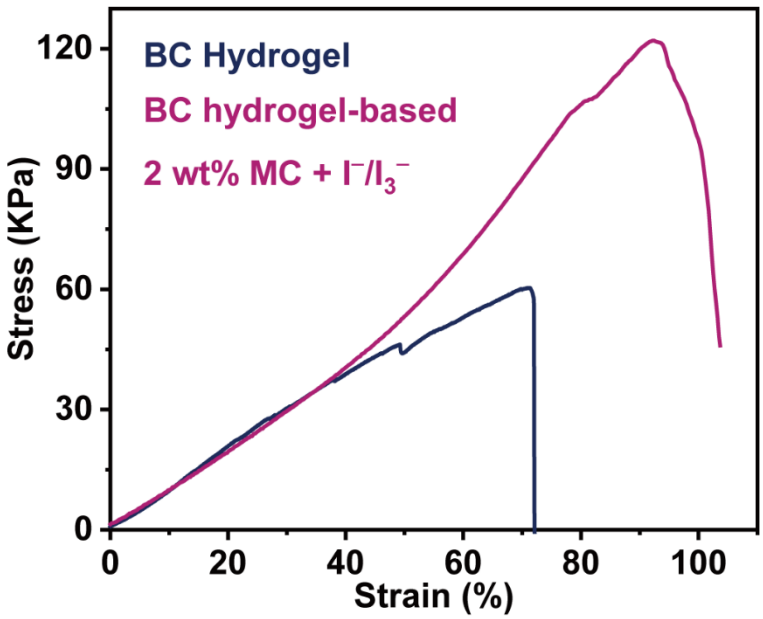

Fig. S16 Tensile stress-strain curves of BC hydrogel and BC hydrogel-based 2 wt% MC + I^-/I_3^- electrolyte, respectively.

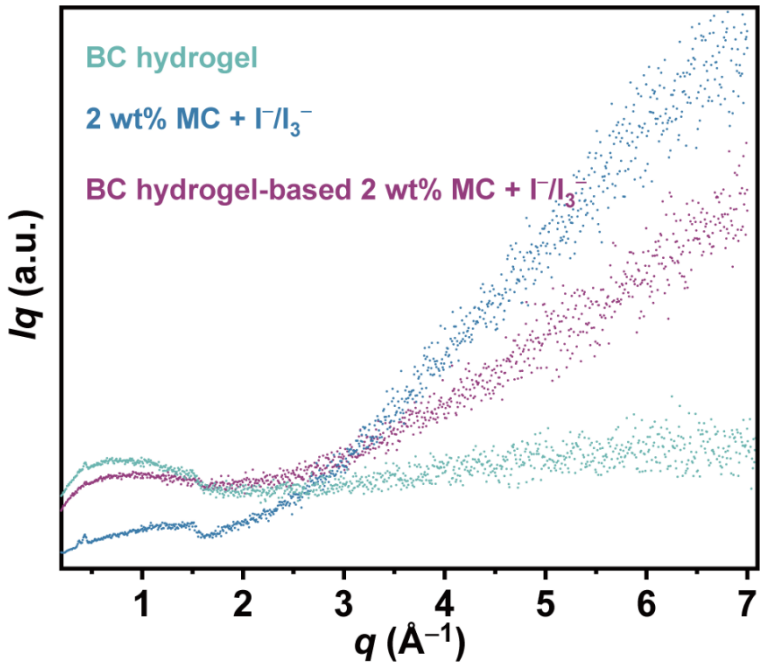

Fig. S17 Representative SAXS profiles of BC hydrogel, 2 wt% MC + I^-/I_3^- and BC hydrogel-based 2 wt% MC + I^-/I_3^- electrolytes under 60 °C, respectively.

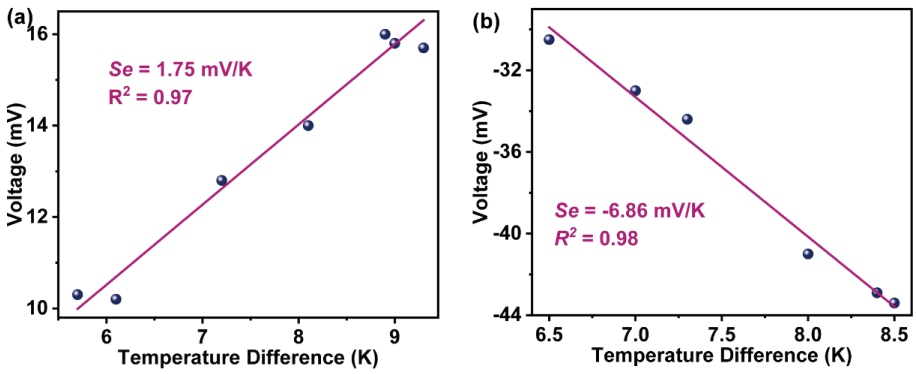

Fig. S18 *Se* for n-type thermocell (a) and p-type thermo-battery (b) with BC hydrogel-based 2 wt% MC + I^-/I_3^- electrolyte, respectively.

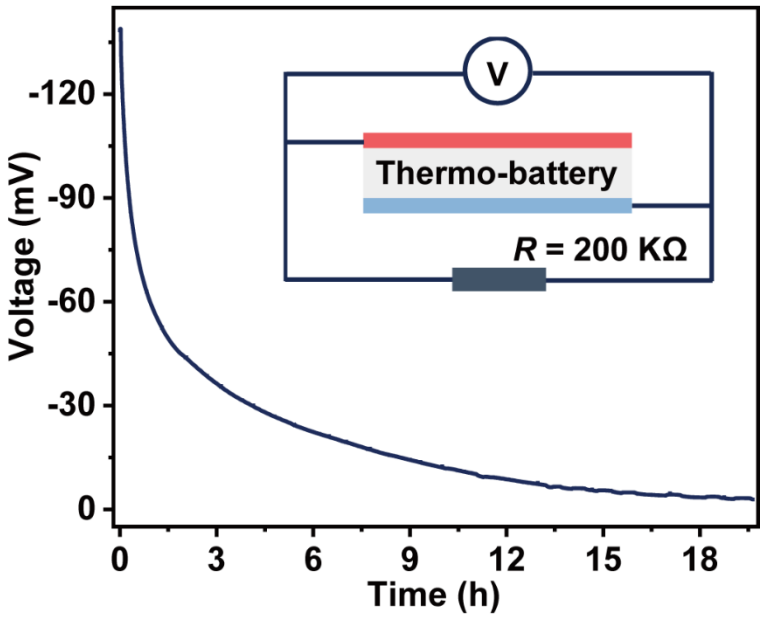

Figure S19. The open-circuit voltage of the continuous discharge process at the external resistor R = 200 kΩ and ΔT = 0 °C. The inset shows the measurement circuit.

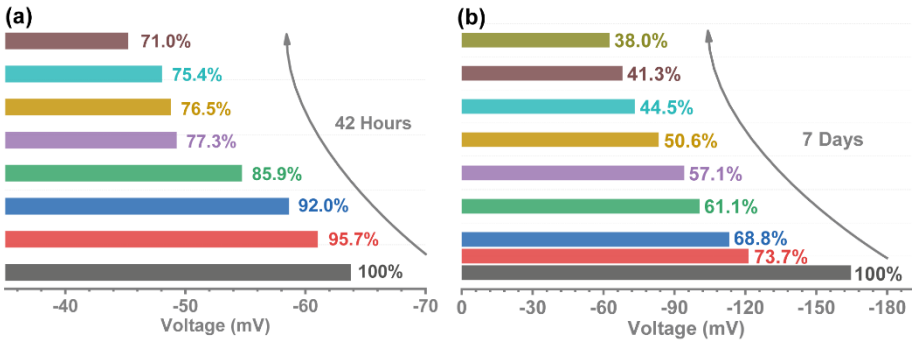

Fig. S20 (a) The V_{OC} attenuation of 2 wt% MC + I^-/I_3^- electrolytes during self-discharging process. The self-discharge time is successively 0, 6, 12, 18, 24, 30, 36 and 42 hours from bottom to top. (b) The V_{OC} attenuation of BC hydrogel-based 2 wt% MC + I^-/I_3^- electrolytes during self-discharging process. The self-discharge time is successively 0, 0.5, 1, 2, 3, 4, 5, 6 and 7 days from bottom to top.

Fig. S21 Photograph of a device module containing 5 units in series.

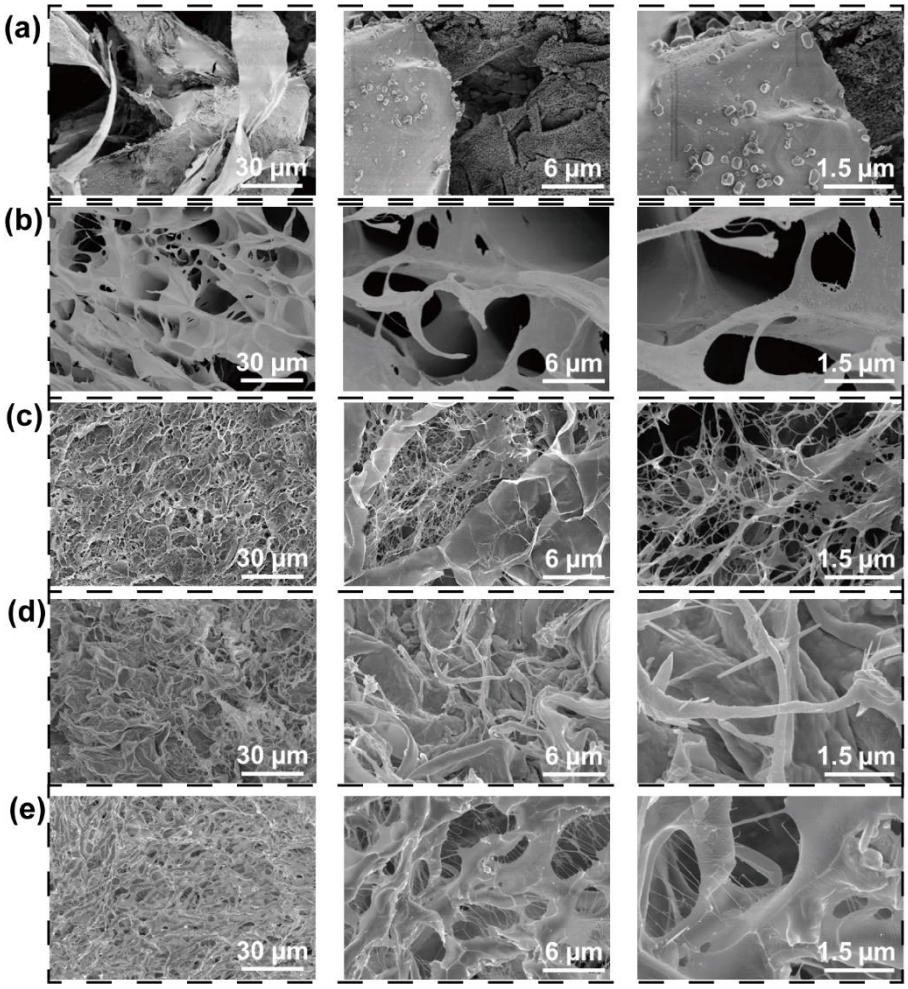

Fig. S22 Morphology characterization of 2 wt% MC + I^-/I_3^- electrolyte with RT (b) and heat (c), BC hydrogel (d), and BC hydrogel-based 2 wt% MC + I^-/I_3^- electrolyte under RT (e) and heating (f) at different magnifications.

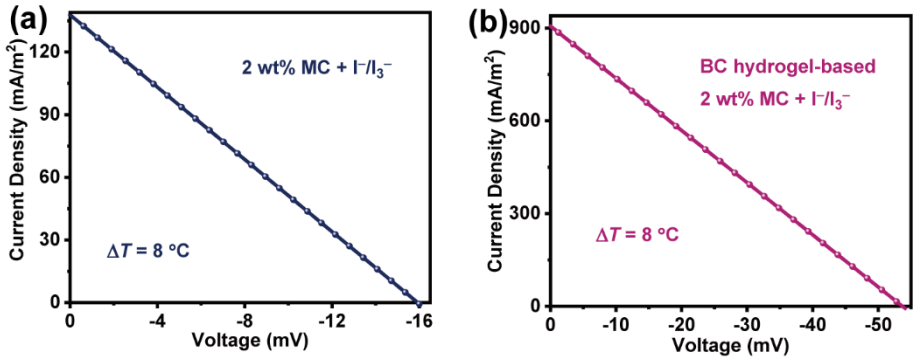

Fig. S23 The output voltage-current density curve of p-type thermo-battery without (a) and with (b) BC hydrogel for 2 wt% MC + I^-/I_3^- electrolyte under ΔT = 8 °C. The cold electrode temperature is fixed at 58 °C.

Table S1. When the hot electrode temperature is below/above the gelation temperature of MC, the reactions at hot and cold electrodes.

n–type	Hot electrode	$I_3^- + 2e^- \rightarrow 3I^-$
	Cold electrode	$3I^- \rightarrow I_3^- + 2e^-$
p–type	Hot electrode	$3I^- \rightarrow I_3^- + 2e^-$
	Cold electrode	$I_3^- + 2e^- \rightarrow 3I^-$

Table S2. Comparison of *Se* values in this work with those reported for I^-/I_3^- based thermocells in the literature.

Redox Couple	State	Hydrophobic Matrix	n/p-type	Se (mV/K)	References
I^-/I_3^-	Liquid	--	n	0.71	[6]
	Liquid	α–cyclodextrins	n	1.45	[5]
	Liquid	Starch	n	1.50	[9]
	Liquid	Poly (N–isopropylacrylamide)	n	0.71	[10]
			p	–1.91	
	Liquid	Poly (N–isopropylacrylamide)	n	0.71	[11]
			p	–1.19	
	Liquid	Methylcellulose	n	1.32	[6]
			p	–1.48	
	Liquid	Methylcellulose	n	1.26	**This work**
			p	–1.83	
	BC Hydrogel		n	1.75	
			p	–6.84	

References

1 W. Zhao, Z. Wang, R. Hu and X. Luo, *EPL (Europhysics Letters)*, 2021, **135**, 26001.

2 Y. Liu, M. Cui, W. Ling, L. Cheng, H. Lei, W. Li and Y. Huang, *Energy Environ.*

Sci., 2022, **15**, 3670–3687.

3 H. Zhou, H. Inoue, M. Ujita and T. Yamada, *Angew. Chem. Int. Ed.*, 2023, **62**, e202213449.

4 H. Wang, S. C. Kim, T. Rojas, Y. Zhu, Y. Li, L. Ma, K. Xu, A. T. Ngo and Y. Cui, *J. Am. Chem. Soc.*, 2021, **143**, 2264–2271.

5 H. Zhou, T. Yamada and N. Kimizuka, *J. Am. Chem. Soc.*, 2016, **138**, 10502-10507.

6 Y. Han, J. Zhang, R. Hu and D. Xu, *Sci. Adv.*, 2022, **8**, eabl5318.

7 B. Yu, J. Duan, H. Cong, W. Xie, R. Liu, X. Zhuang, H. Wang, B. Qi, M. Xu, Z. L. Wang and J. Zhou, *Science*, 2020, **370**, 342–346.

8 S. Sahami and M. J. Weaver, *J. Electroanal. Chem.*, 1981, **122**, 155–170.

9 H. Zhou, T. Yamada and N. Kimizuka, *Sustain. Energ. Fuels*, 2018, **2**, 472–478.

10 J. Duan, B. Yu, K. Liu, J. Li, P. Yang, W. Xie, G. Xue, R. Liu, H. Wang and J. Zhou, *Nano Energy*, 2019, **57**, 473–479.

11 X. Shen, J. Wu, Z. Hua and G. Liu, *ACS Appl. Energy Mater.*, 2023, **6**, 10147–10154.